Strategic self-limiting production of infectious HIV particles by CRISPR in permissive cells

Hong Liu,[1,7] Chen Chen,[1,7] Shuren Liao,[1] Danielle K. Sohaii,[2] Conrad R.Y. Cruz,[2] Tricia H. Burdo,[1] Thomas J. Cradick,[3] Anand Mehta,[4] Carlos Barrero,[5] Magda Florez,[5] Jennifer Gordon,[3] Stephane Grauzam,[4] James Dressman,[4] Shohreh Amini,[6] Catherine M. Bollard,[2] Rafal Kaminski,[1] and Kamel Khalili[1]

[1]Center for Neurovirology and Gene Editing, Department of Microbiology, Immunology, and Inflammation, Lewis Katz School of Medicine at Temple University, 3500 N. Broad Street, 7th Floor, Philadelphia, PA 19140, USA; [2]Center for Cancer and Immunology Research, Children's National Health System, The George Washington University, 7144 13th Place NW, Washington, DC 20012, USA; [3]Excision Biotherapeutics, Inc., 499 Jackson Street, San Francisco, CA 94111, USA; [4]Department of Cell and Molecular Pharmacology, Medical University of South Carolina, Basic Science Building, Room 310, 173 Ashley Avenue, Charleston, SC 29425, USA; [5]Department of Pharmaceutical Sciences, School of Pharmacy, Temple University, 3307 N. Broad Street, Philadelphia, PA 19140, USA; [6]Department of Biology, College of Science and Technology, Temple University, 1900 North 12th Street, Philadelphia, PA 19122, USA

Post-translational glycosylation of the HIV-1 envelope protein involving precursor glycan trimming by mannosyl oligosaccharide glucosidase (MOGS) is critically important for morphogenesis of virions and viral entry. Strategic editing of the MOGS gene in T lymphocytes and myeloid origin cells harboring latent proviral DNA results in the production of non-infectious particles upon treatment of cells with latency reversal agents. Controlled activation of CRISPR-MOGS by rebound HIV-1 mitigates production of infectious particles that exhibit poor ability of the virus to penetrate uninfected cells. Moreover, exclusive activation of CRISPR in cells infected with HIV-1 alleviates concern for broad off-target impact of MOGS gene ablation in uninfected cells. Combination CRISPR treatment of peripheral blood lymphocytes prepared from blood of people with HIV-1 (PWH) tailored for editing the MOGS gene (CRISPR-MOGS) and proviral HIV-1 DNA (CRISPR-HIV) revealed a cooperative impact of CRISPR treatment in inhibiting the production of infectious HIV-1 particles. Our design for genetic inactivation of MOGS by CRISPR exhibits no detectable off-target effects on host cells or any deleterious impact on cell survival and proliferation. Our findings offer the development of a new combined gene editing-based cure strategy for the diminution of HIV-1 spread after cessation of antiretroviral therapy (ART) and its elimination.

INTRODUCTION

Entry of human immunodeficiency virus type-1 (HIV-1) to host cells, including T lymphocytes and myeloid lineage cells, is a multistep process that begins with the interaction of the glycosylated viral envelope protein, gp120 (Env), with host cell receptors, CD4, and co-receptors, including CCR5 and CXCR4,[1,2] followed by fusion of viral and host cell membranes,[3] internalization of the virion, and release of its genomic RNA in the cytoplasm.[4] Both gp120 and gp41 subunits of HIV-1 Env are N-linked glycosylated, with 28 of 32 potential N-linked glycosylation sites (PNGs) located in gp120.[5–8] The extensive glycosylation of Env shields the viral envelope protein from recognition by host neutralizing antibodies.[9–12] N-linked glycosylation is a multistep post-translational process in which a high mannose-type sugar chain ($Glc_3Man_9GlcNAc_2$) is engaged with an asparagine residue in the context of the conserved motif Asn-X-Ser/Thr, where X can be any amino acid except proline.[13] This intracellular chemical modification is followed by trimming of glucose and mannose residues and adding terminal sugars to constitute a complex-type glycan as the glycoprotein structurally matures through the endoplasmic reticulum (ER) and Golgi along cellular secretory pathways.[13,14] MOGS (mannosyl oligosaccharide glucosidase) is the ER-resident enzyme of the N-linked glycosylation pathway responsible for the removal of the first glucose residue from the precursor glycan an indispensable step required for further trimming and re-decoration of glycan chains of nascent glycoprotein in ER-lumen before turning to Golgi apparatus in the cytosol (Figure S1A). These observations prompted us to postulate that ablation of the MOGS gene by CRISPR gene editing either alone or in combination with CRISPR-mediated editing of HIV-1

Correspondence: Rafal Kaminski, Center for Neurovirology and Gene Editing, Department of Microbiology, Immunology, and Inflammation, Lewis Katz School of Medicine at Temple University, 3500 N. Broad Street, 7th Floor, Philadelphia, PA 19140, USA.
E-mail: rafalkim@temple.edu
Correspondence: Kamel Khalili, Center for Neurovirology and Gene Editing, Department of Microbiology, Immunology, and Inflammation, Lewis Katz School of Medicine at Temple University, 3500 N. Broad Street, 7th Floor, Philadelphia, PA 19140, USA.
E-mail: kamel.khalili@temple.edu
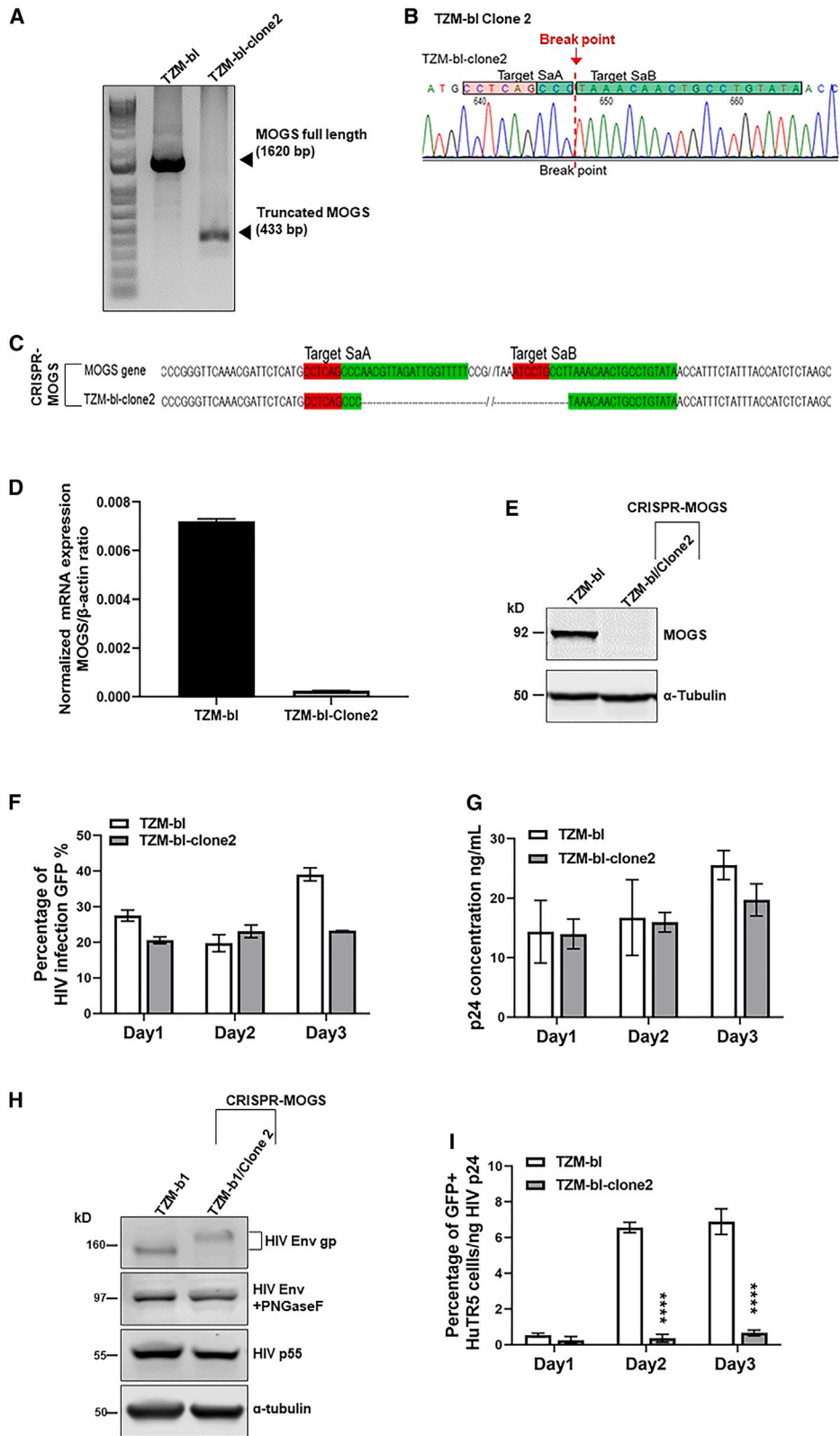
(legend on next page)

proviral DNA mitigates the production of fully infectious particles from the primary cells (Figure S1B).

RESULTS

Inactivation of MOGS by CRISPR gene editing

The initial bioinformatic assessment of the human *MOGS* gene sequence led to the identification of two potential binding sites for CRISPR gRNAs, designated A and B (Figures S2A and S2B) with high on-target and minimum, if any, nominated off-target activity in the host genome (Table S1). Protospacer regions of these gRNAs were sequentially cloned into "all-in-one" AAV-delivery SaCas9 pX601 vector, hereafter referred to as CRISPR-MOGS (Figure S2C), and expression of each gRNA and SaCas9, and the excision of the *MOGS* gene was verified (Figures S2D and S2E).

To assess the importance of MOGS in the genesis of infectious virions, in the first proof-of-principle experiments, we used the TZM-bl cells, a HeLa-CD4/CCR5/CXCR4 laboratory cell model that supports viral replication.[15,16] CRISPR-MOGS-treated TZM-bl cells were clonally expanded and single-cell clones with a complete knockout of the *MOGS* gene were identified. The introduction of CRISPR-MOGS plasmid to TZM-bl cells resulted in the precise removal of the assigned DNA fragment spanning between the A and B target sites in the *MOGS* gene (Figure 1A) and was verified using Sanger DNA sequencing (Figures 1B and 1C). As expected, results from the RNA and protein detection assays showed a lack of expression of the *MOGS* gene (Figures 1D and 1E). Investigation of HIV-1 replication by detecting the reporter GFP marker protein in the HIV-1$_{NL4-3-GFP-P2A-nef}$-infected cells (Figure 1F), and the Gag p24 viral protein levels in the culture media of the primary infection (Figure 1G) indicated that initially (days 1 and 2) the elimination of MOGS in TZM-bl had virtually no impact on the primary infection. At day 3 post-infection, virus levels in MOGS+ cells increased while its levels in MOGS− cells remain unchanged. Under similar experimental conditions, it was noted that the viral progenies from the MOGS− cells are incapable of replicating in the secondary infection, suggesting that aberration in trimming of heavily glycosylated viral gp120 in the absence of MOGS results in the production of the larger size of viral glycoprotein (Figure 1H), which is associated with the decline in the viral infectivity (Figure 1I). Importantly, as shown in Figures S3 and S4 and Table S1, the introduction of CRISPR-MOGS to TZM-bl cells had no impact on the top five bioinformatically nominated off-target sites in the human genome. Also, no adverse effects on cell viability and growth rate (Figures S5A–S5D; also see Table S3), the progression

through the cell cycle, and apoptosis were noted in MOGS− T lymphoid and myeloid cells (Figures S6A–S6D; also see Table S3).

Impact of CRISPR-MOGS treatments on secondary infection of HIV-1 in T lymphocytes and latently infected myeloid cells

As CD4+ T cells are the major targets for HIV-1, we verified the effects of MOGS knockout on HIV-1 infection of Jurkat T-lymphoid cell line and primary CD4+ T cells. Similarly, as observed in MOGS− TZM-bl cells, HIV-1 infection of MOGS− Jurkat cells resulted in a shift in the size of the viral envelope glycoprotein (Figure 2A; also see Figure 1H), with no impact on the level of the viral p55 capsid protein and no drastic effect on the primary viral infection (Figures 2B and 2C). However, viral progeny produced in these cells was completely non-infectious (Figure 2D). This result once again points to the importance of MOGS in the genesis of infectious viral particles.

We then used primary human CD4+ T cells isolated from the peripheral blood of healthy donors. Cells were electroporated with CRISPR ribonucleoprotein complexes composed of Cas9 and four different gRNAs (MOGS#1–4) targeting the coding sequence of the *MOGS* gene and then infected with HIV-1$_{NL4-3-Bal-GFP}$. The genomic DNA and protein analyses revealed that treatment of cells with gRNAs MOGS#1 and #4, which showed the highest on-target indel knockout scores (Figure S7), led to the most profound decrease in MOGS protein level (Figure 2H) compared with control or gRNA MOGS#2 and #3 treated cells. Importantly, similarly, as in the cell line experiments, we did not observe differences in primary infection levels in RNP-CRISPR-MOGS-treated CD4+ T cells compared with control cells (Figures 2F and 2G). On the other hand, the virus present in the supernatants from these cells was significantly less infective in the second round of infection using target HutR5 cells (Figure 2H). Furthermore, the secondary infection levels correlated with the levels of MOGS expression observed in primary CD4+ T cells, i.e., more MOGS protein expression (Figure 2E, #2 and #3), the less suppression of viral presence in the secondary infection (Figure 2H, #2 and #3).

Recently, myeloid cells have received more attention because of their potential role in the pathogenesis of HIV infection in hosting/maintaining HIV-1 in the latent stage.[17,18] Here, we found that treatment of the latently infected myeloid cells (U1) with CRISPR-MOGS followed by reactivation of the latent HIV-1 using PMA plus the HDAC inhibitor Vorinostat (SAHA) showed a clear shift in the size

Figure 1. Editing of the *MOGS* gene by CRISPR affects the infectivity of the viral progeny derived from MOGS− cells

(A) PCR genotyping results of CRISPR-Cas9-mediated excision of an exon 1 and 2 region of the MOGS gene in clone 2 of TZM-bl cells. WT TZM-bl cells were used as a control. The arrows point to intact full-length 1,620-bp-long MOGS promoter-intron 3 amplicon (top arrow) and CRISPR-cleaved/end-joined 433 bp truncated amplicon (bottom arrow), carrying 1,187 bp deletion of the exon 1 and 2 region of the MOGS gene. (B) Sanger sequence tracing of truncated CRISPR-cleaved/end-joined amplicons detected for MOGS− TZM-bl clone 2. (C) Sequence alignment of the same sequences. gRNAs target sites are highlighted in green and PAM sequences in red. (D) qRT-PCR analysis of MOGS mRNA levels in WT and MOGS− clone 2 TZM-bl cells. β-Actin mRNA was used as a reference gene. (E) Immunoblot analysis of MOGS protein expression in the same cells. α-tubulin was used as a loading control. (F) GFP-flow cytometry analysis of HIV-1$_{NL4-3-GFP}$ infection in WT and MOGS− clone 2 TZM-bl cells. (G) HIV-1 gag p24 ELISA results for supernatants collected from the same cells. (H) Immunoblot analysis of HIV-1 gp160 in infected WT and MOGS− clone 2 TZM-bl cells. PNGaseF digestion was used to remove glycans from glycoproteins in lysates. HIV-1 p55 and α-tubulin were used as infection and loading controls, respectively. (I) GFP-flow cytometry analysis of HutR5 T-lymphoid cells infected with supernatants derived from HIV-1$_{NL4-3-GFP}$-infected cells from (G). Student's t test (two-tailed) was used in (I). ****p < 0.0001.
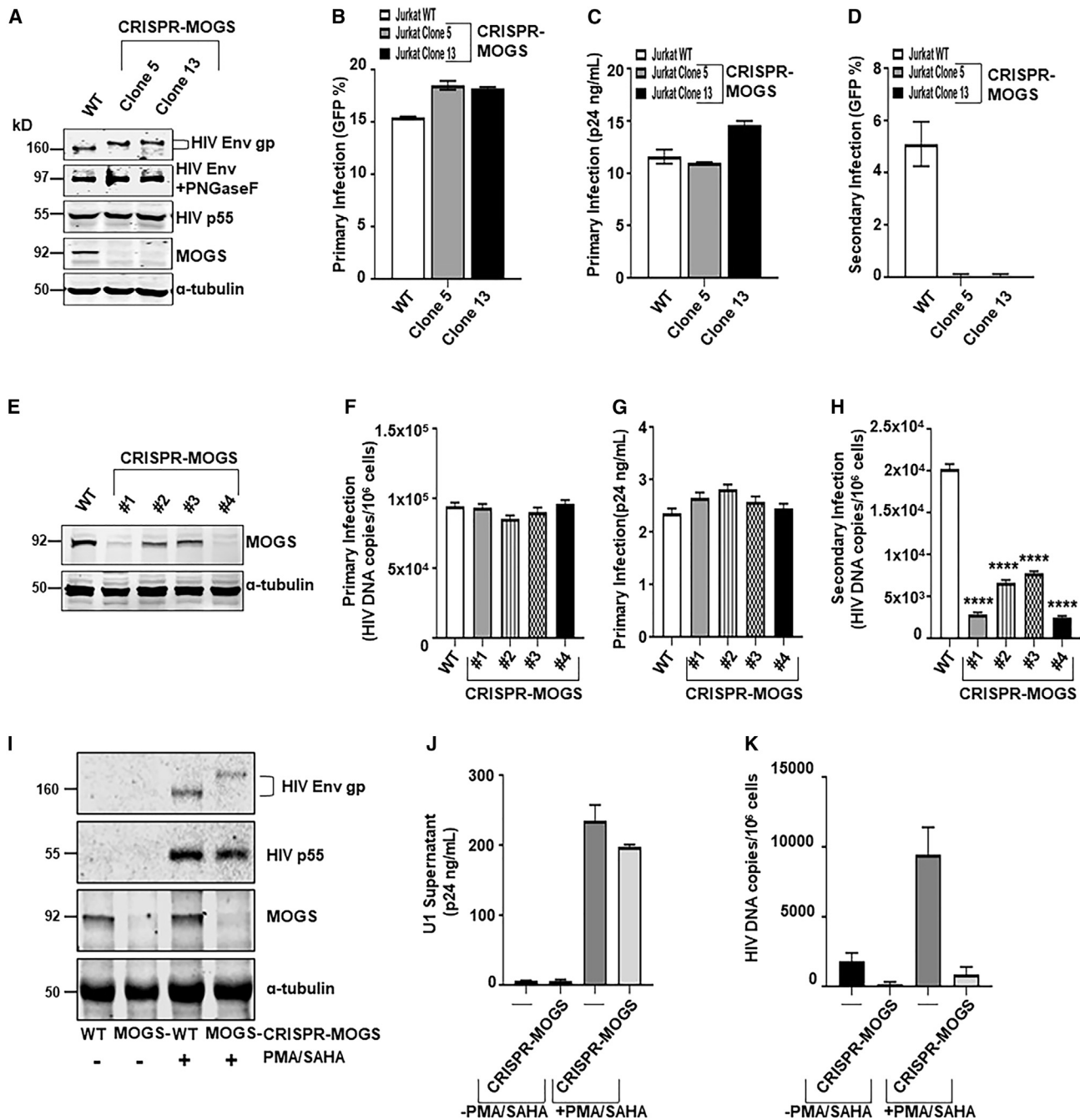
Figure 2. The *MOGS* gene knockout in T and monocytic cells results in the production of infection-defective progeny virions

(A) Immunoblot analysis of HIV-1 gp160 and MOGS in HIV−1$_{NL4-3-GFP}$-infected WT and MOGS− clone 5 and 13 Jurkat cells. HIV-1 p55 and α-tubulin were used as infection and loading controls. (B) GFP-flow cytometry analysis of HIV-1$_{NL4-3-GFP}$ infection in WT and MOGS− clone 5 and 13 Jurkat cells. (C) HIV-1 gag p24 ELISA results for supernatants collected from the same cells. (D) GFP-flow cytometry analysis of HutR5 T-lymphoid cells infected with supernatants derived from HIV-1$_{NL4-3-GFP}$-infected WT and MOGS− clone 5 and 13 Jurkat cells. (E) Immunoblot analysis of MOGS in primary human CD4+ T cells electroporated with RNP-CRISPR-Cas9/MOGSgRNA #1, #2, #3, or #4 complexes. WT cells were used as a control. α-tubulin was used as a loading control. (F) ddPCR quantification of viral DNA in HIV-1$_{NL4-3-GFP}$-infected cells from (E). (G) HIV-1 gag p24 ELISA results for supernatants collected from HIV-1$_{NL4-3-GFP}$ infected primary human CD4+ T cells. (H) ddPCR quantification of viral DNA in HutR5 T-lymphoid cells infected with supernatants derived from HIV-1$_{NL4-3-GFP}$ infected WT and RNP-CRISPR-Cas9/MOGSgRNA #1, #2, #3, or #4 treated primary human CD4+ T cells. (I) Immunoblot analysis of HIV-1 gp160 and MOGS in uninduced or PMA/SAHA-treated U1 WT and MOGS− cells. HIV-1 p55 and α-tubulin were used as infection and loading controls. (J) HIV-1 gag p24 ELISA results for supernatants collected from cells in (I). (K) ddPCR quantification of viral DNA in HIV-1 permissive HutR5 T-lymphoid cells infected with supernatants derived from cells in (I). One-way ANOVA and Dunnett's multiple comparisons test was used in (H). ****p < 0.0001.
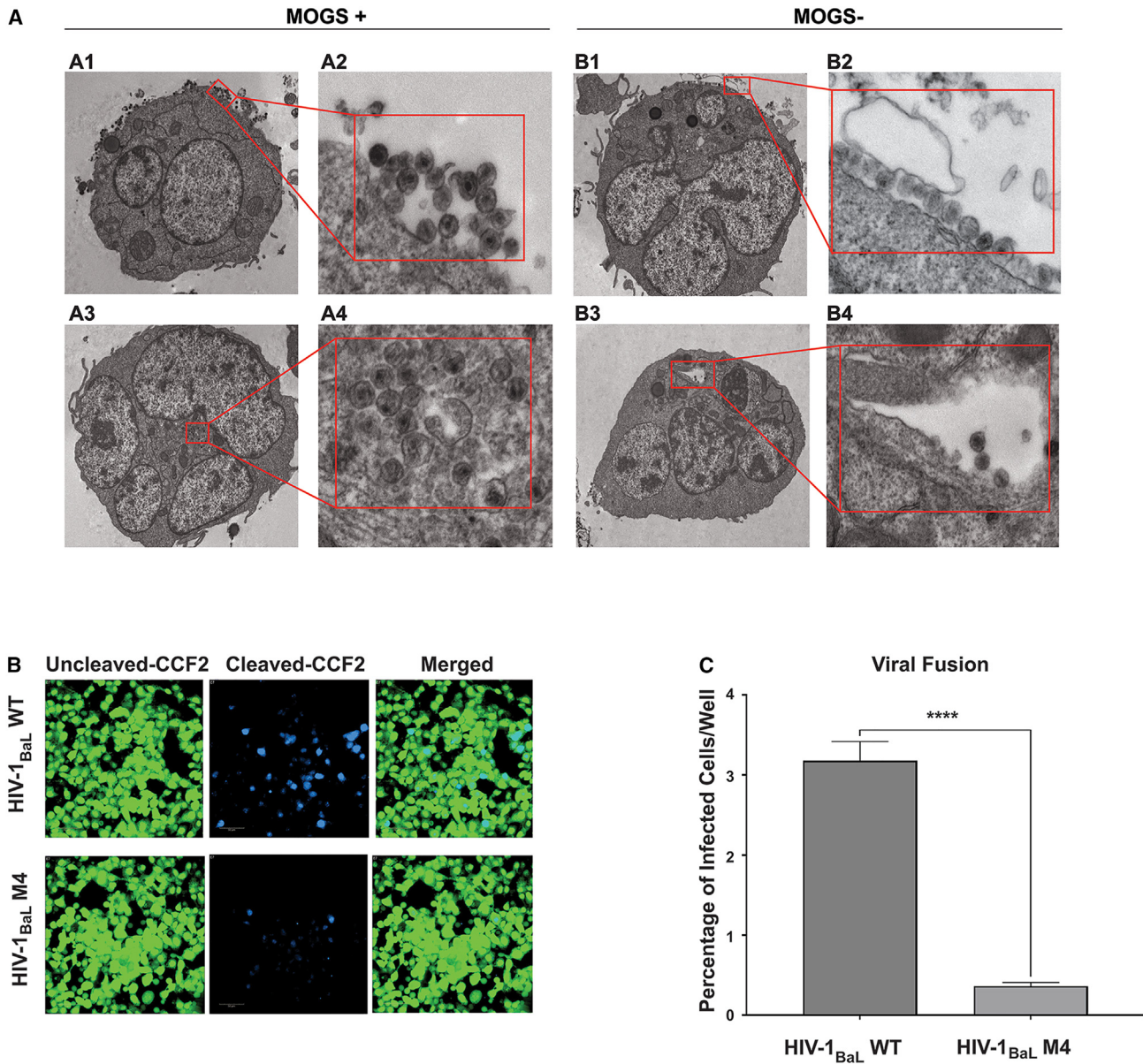
Figure 3. Viral particles released from MOGS− cells fail to enter uninfected T cells

(A) Electron microscopy images of HutR5 cells incubated for 1 h with equal titers of virus-containing supernatants derived from WT (A1–A4) or MOGS− (B1–B4) J1.1 cells. Original images with scale bars and acquisition details are shown in Figure S8. (B) Images of TZM-bl cells loaded with the CCF2-AM BlaM substrate after inoculation with HIV virus bearing the BlaM-Vpr chimera produced from HEK293T WT cells or MOGS− cells (clone 4). Cells were identified by CCF2-AM signal (488/555nm, green), and viral entry was detected by intracellular processed-CCF2 signal (400/430nm, blue). Scale bars 50 mm. (C) Bar graph showing the percentage of viral entry (cleaved-CCF2-positive) with respect to the total number of cells per well (uncleaved-CCF2-AM-positive). ****$p < 0.0001$. Data were analyzed using the two-tailed unpaired t test, using Prism software.

of the viral envelope glycoprotein produced in CRISPR-MOGS-treated U1 cells, indicative of misconfiguration of glycans of the viral envelope protein emerged from the MOGS− myeloid cells (Figure 2I). As before, treatment did not affect the level of viral production in the parental cells, yet the reactivated viral particles were incapable of spreading and completing secondary infection in naive, permissive HutR5 cells (Figures 2J and 2K).

On the basis of the fact that the persistent HIV-1 reservoir responsible for the virus reemergence upon antiretroviral therapy (ART) interruption is predominantly composed of latently infected resting memory CD4^{+} T cells,[19] in the next set of experiments, we used two well-characterized HIV-1 latency T cell line models: ACH-2 and J1.1 cells.[20–22] Same as before, cells were treated with CRISPR-MOGS, and single-cell MOGS− clones were identified (Figure 4A). In
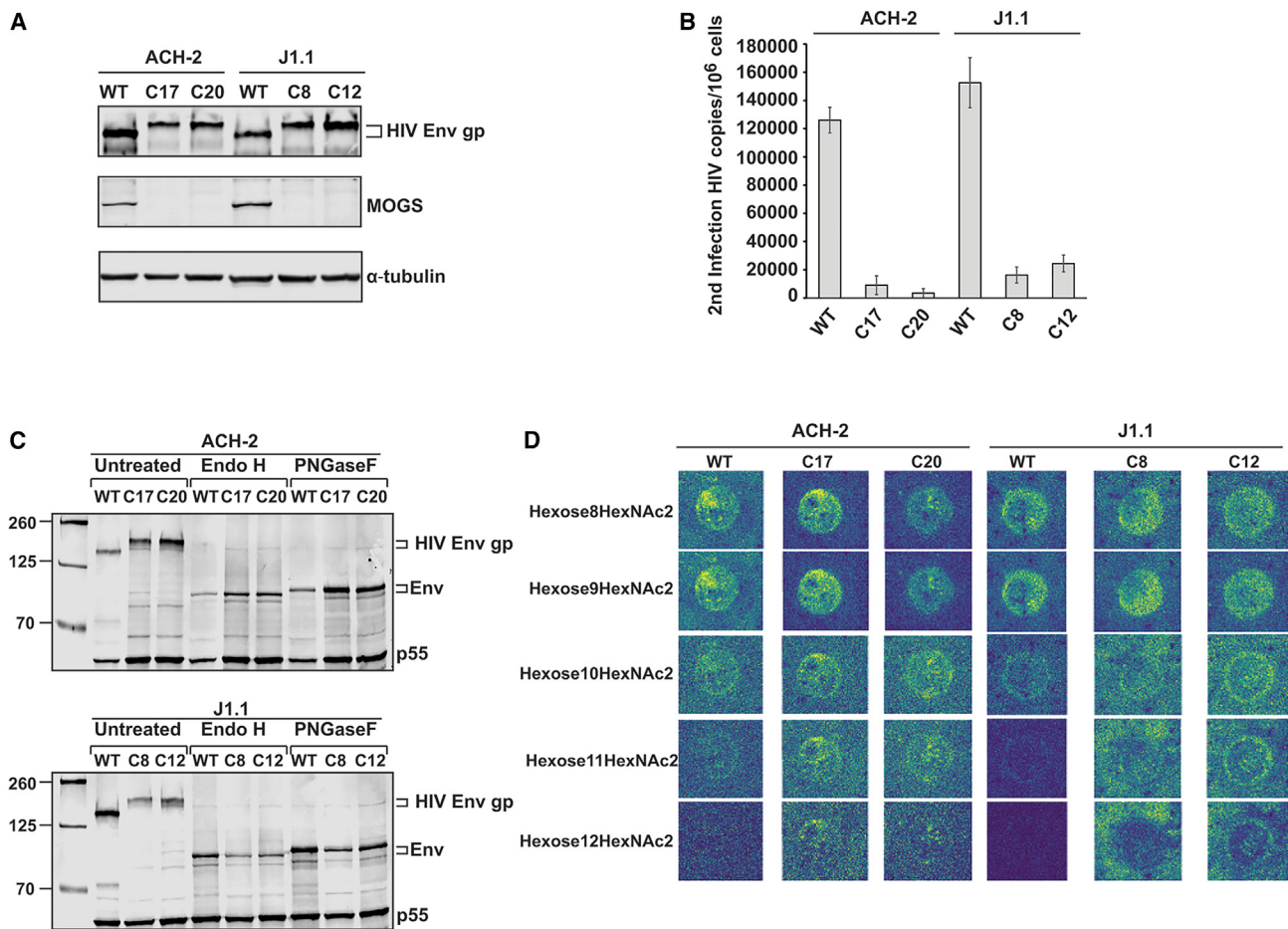
Figure 4. Upon latency reversal, virions released from MOGS− latently infected T cells show residual infectivity and contain hyper-glycosylated (unprocessed) glycans

(A) Immunoblot analysis of HIV-1 gp160 and MOGS expression in WT and MOGS− ACH-2 and J1.1 latently infected T cell lines upon PMA/SAHA (ACH-2) or TNF-α (J1.1) treatment. α-Tubulin was used as the loading control. (B) ddPCR analysis of genomic DNA extracted from HutR5 cells treated with supernatants derived from cells from (A). (C) Immunoblot analysis of HIV-1 gp160 in the untreated or treated with Endo H or PNGaseF protein lysates prepared from WT and MOGS− ACH-2 and J1.1 cells (same as in A). HIV-1 p55 was used to show viral protein expression levels. (D) Viral particles from supernatants of PMA/SAHA or TNF-α-treated wild-type cells (ACH- 2 and J1.1) or MOGS− (ACH-2 C17 and C20, J1.1, C8, and C12) cells were purified and analyzed using MALDI-glycan imaging.[24] N-linked glycan consisting of large structures with m/z values corresponding to Hexose11HexNAc2 (m/z = 2,279.7400) and Hexose12HexNAc2 (m/z = 2,391.7929) were observed only in the MOGS− cells.

follow-up studies, supernatants from MOGS+ and MOGS− cells were collected and used to infect lymphocytes. In the first study, HutR5 T cells were incubated for 1 h with equal titers of virus obtained from the supernatants collected from MOGS+ and MOGS− J1.1 cells (300 ng Gag p24/10^7 cells) and, after fixing, analyzed using electron microscopy for the presence of cell membrane-associated virions. Viral particles obtained from MOGS+ cells are scattered around the cell membrane (Figure 3A, sub-panels A1 and A2; also see Figures S8A and S8B), and that a large number of viral particles are detected in the cytoplasm, suggesting successful viral entry (Figure 3A, sub-panels A3 and A4; also see Figures S8C and S8D). In several instances, the attachment of the virus to the target cells was clearly detected (see Figure S8). Interestingly, we observed an unusual assembly of viruses obtained from MOGS− cells, as they appeared to

be lined up outside of the uninfected cells (Figure 3A, sub-panels B1 and B2; also see Figures S8E and S8F). Furthermore, many of the cells exhibited the limited presence of the virus inside of the cells (Figure 3A, sub-panels B3 and B4; also see Figures S8G and S8H). These results are in accord with the observations in Figure 2, pointing to the weak infectivity of HIV particles produced in the MOGS− cells. To further investigate the viral entry step, we performed a sensitive and specific enzyme-based assay allowing quantitative measurement of virion entry by fusion, Vpr-β-lactamase assay.[23] In this assay β-lactamase-Vpr chimeric proteins (BlaM-Vpr) are incorporated during packaging into HIV-1 virions and subsequently delivered into the cytoplasm of the target cells upon successful fusion-dependent viral entry. Prior to infection, target cells are loaded with a fluorescent substrate of β-lactamase (BlaM), the CCF2 dye which is cleaved by BlaM,
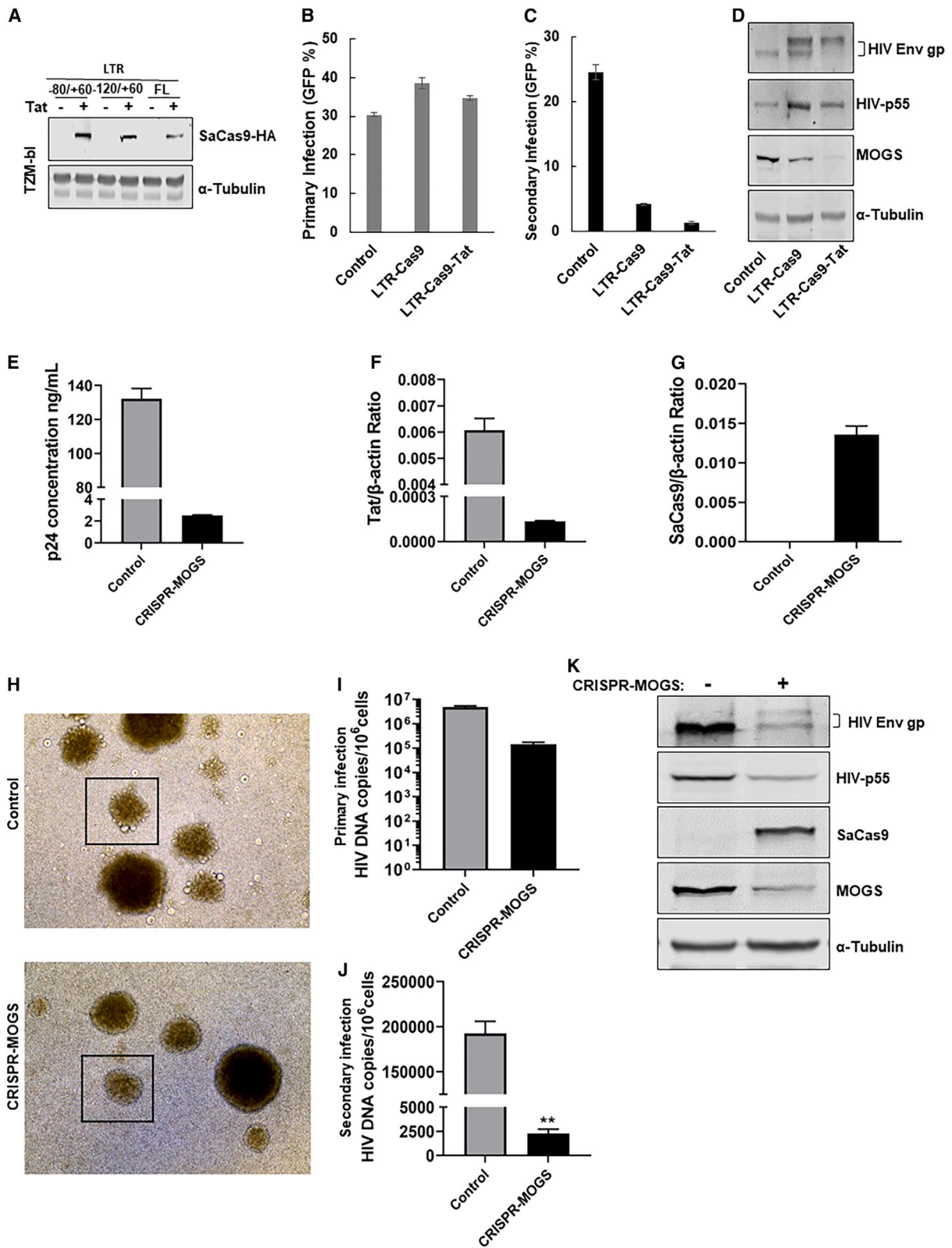
(legend on next page)

changing the fluorescence emission spectrum from green (520 nm) to blue (447 nm) and thereby allowing viral entry to be detected by fluorescence microscopy. Results from this assay (Figures 3B and 3C) showed significantly lower levels of viral entry by HIV-1 virions collected from the MOGS− cells compared with those that are prepared from the MOGS+ cells under comparable conditions (Figures 3B and 3C; also see Figure S9). Altogether, the results from electron microscopy and viral entry assays point to the inability of the virus derived from the MOGS− cells to penetrate uninfected cells which result in a block of HIV-1 infection cycle and virus spread.

Next, we investigated the state of HIV-1 Env glycosylation and the importance of MOGS in the infectivity of emerging rebound viruses using MOGS− J1.1 and ACH-2 cells. The lack of MOGS expression and the subsequent shift in the size of viral envelope protein upon virus reactivation with latency reversal drugs was confirmed using western blot (Figures 4A, 4C, and S10). Results from secondary infection verified a drastic decline in the infectivity of the rebound virus that was reactivated in cells with no MOGS expression (Figure 4B). Furthermore, the differences in molecular weight depended on N-glycosylation pattern, as revealed after N-glycan removal by pretreatment of protein lysates with Endo H that removes glycan and PNGase F that removes N-linked oligosaccharides from glycoprotein (Figure 4C; also see Figure S10).

Subsequently, the glycan analysis of the viruses purified from the MOGS− cells was performed. Purified virus (see materials and methods) was spotted onto nitrocellulose as described previously.[25] Subsequently, glycan attached to the virus was analyzed by matrix-assisted laser desorption ionization (MALDI)-glycan imaging. Although complex glycans were detected in all samples (data not shown), large glycans containing ≥10 hexoses with only two HexNAcs were observed only on viruses produced in MOGS− cells (Figure 4D). On the basis of the observed m/z values (2,279.7400 and 2,391.7929), these glycans are presumed to be a Glc3Man8 and a Glc3Man9 glycan, which is the result of the inhibition of glucosidase 1 and 2. Additionally, the impact of MOGS deletion on the total glycan profile on cell level was determined by MALDI-glycan imaging. Briefly, MOGS+ (J), MOGS− (JM) J1.1 cells and MOGS+ (U), MOGS− (UM) U1 cells were precipitated onto amine reactive slides

as described previously,[26] and the glycosylation was determined following application of PNGase F PRIME and MALDI imaging.[27] We also observed large glycans containing ≥10–12 hexoses with only two HexNAcs remaining in MOGS− cells (Figure S11). On the basis of the canonical rules of N-linked glycosylation, the structure in Figure S11A, with a m/z of 2,391.7929, is a glycan composed of 12 hexoses and 2 HexNAc, and would presumably have a structure of a Glc3Man9GlcNAc2 glycan. Similarly, the glycans found in Figures S11B and S11C correspond to Glc3Man8GlcNAc2 and Glc3Man7GlcNAc2 glycan. The relative contribution of different types of glycans to cell surface glycome of wild-type (WT) and MOGS− cells is summarized in Figures S11D–S11G. It is noted that glycan processing still occurred in these cells (Figures S11F and S11G) and resulted in the formation of complex glycan, presumably, through the use of the Golgi endo-α-mannosidase pathway.[28]

Strategic activation of CRISPR-MOGS by HIV-1 results in the diminution of infectious particles

To restrict the editing of the *MOGS* gene to the HIV-1 infected cells, we employed the strategy that triggers activation of CRISPR-MOGS and the expression of its Cas9 endonuclease by the HIV transcription trans-activator Tat.[29] In the first set of experiments, we demonstrated that a minimal sequence of the HIV-1 long terminal repeat (LTR) promoter spanning −80 to +60 of the LTR remains responsive to Tat protein in HEK293T cells (Figure S12A). Next, we showed that Tat-mediated induction of CRISPR-MOGS results in the appearance of larger size envelope proteins (Figure S12B) because of aberrant glycan trimming and production of virions that are less infectious during secondary infection (Figure S12D). Importantly, HIV-1 infection-derived Tat was sufficient to induce these changes (Figure S12B, middle line). However, the level of the aberrantly glycosylated viral envelope was higher upon overexpression of Tat (Figure S12B, third line). Again, no impact on the primary infection (Figure S12C) was observed. In subsequent studies, we found that similar to HEK293T cells, Tat-mediated expression of SaCas9 in TZM-bl cells (Figure 5A), by potentiating CRISPR-MOGS, results in the diminution of MOGS protein and the appearance of the shifted (larger size) band, indicative of aberrant trimming process of the viral envelop protein glycans in the absence of MOGS in the infected cells (Figure 5D). This cascade of events leads to the production of viral progeny with a significantly

Figure 5. Treatment of primary PWH-derived CD4+ T cells with Tat-inducible CRISPR-MOGS vector leads to self-limiting viral rebound and blocks the spread of HIV infection

(A) Immunoblot analysis of SaCas9-HA expression in TZM-bl cells transfected with pLTR−80/+60-SaCas9-MOGS, pLTR−120/+60-SaCas9-MOGS, or pLTR−454/+60-SaCas9-MOGS constructs together with empty pCMV (Tat−) or pCMV-Tat (Tat+) plasmids. α-Tubulin was used as an internal control. (B) GFP-flow cytometry analysis of HIV$_{NL4-3-GFP}$-infected cells. (C) GFP-flow cytometry analysis of HutR5 T-lymphoid cells infected with supernatants derived from infected cells shown in (B). (D) Immunoblot analysis of gp160 in HIV-1$_{NL4-3-GFP}$-infected TZM− bl cells untransfected (control) or transfected with pLTR−80/+60 SaCas9-MOGS in the absence or presence of Tat-expressing plasmid. HIV-1 p55 and α-tubulin were used as infection and loading controls. (E) HIV-1 Gag p24 ELISA results from supernatants of control or LV-LTR−80/+60-SaCas9-MOGS-treated primary CD4+ T cells of ART-suppressed patient living with HIV (PLWH). CD4+ T cells were isolated from frozen PBMCs and were stimulated with anti-CD3 and anti-CD28 antibodies to stimulate latent HIV-1 for three days. Next cells were transduced with lentivirus expressing CRISPR-LTR−80/+60-SaCas9-MOGS and viral load was assessed after 12 days. (F) qRT-PCR results showing the mRNA expression levels of HIV-1 Tat and (G) SaCas9. (H) Light microscopy images of control (top) or LV-LTR−80/+60-SaCas9-MOGS-treated (bottom) primary CD4+ T cells (100×). (I) ddPCR quantification of intracellular viral DNA in control and LV- LTR−80/+60-SaCas9-MOGS-treated PWLH-derived CD4+ T cells. (J) ddPCR quantification of intracellular viral DNA in the HutR5 cells treated with supernatants derived cells in E. (K) Immunoblot analysis of HIV-1 gp160, SaCas9-HA, and MOGS protein expression in control and LV-LTR−80/+60-SaCas9-MOGS-treated PWLH-derived CD4+ T cells. HIV-1 p55 and α-tubulin were used as infection and loading controls. Unpaired t test (two-tailed) was used in (E), (F), and (J). **p < 0.01.
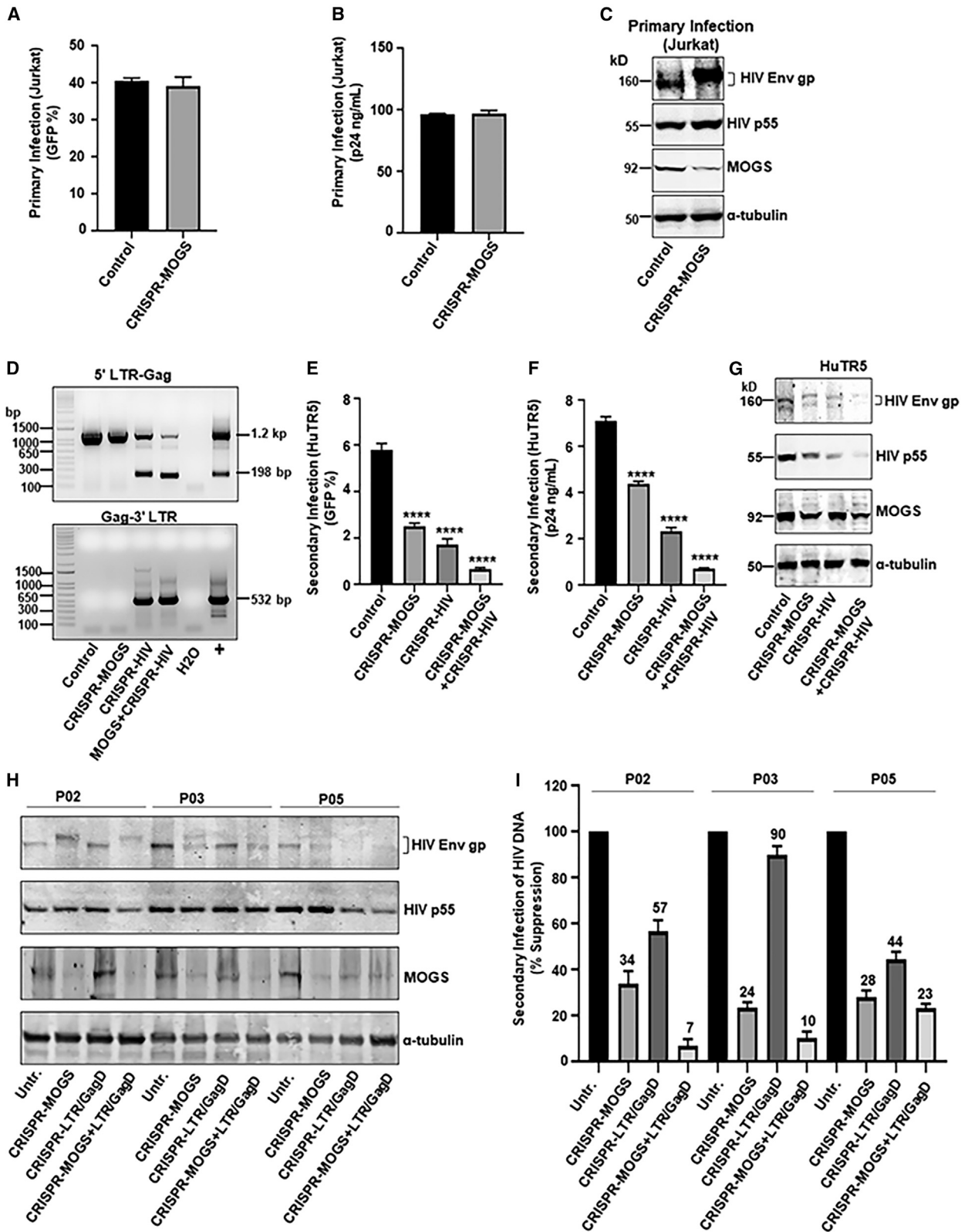
(legend on next page)

reduced level of infectivity in permissive cells (Figure 5C). As before, no significant effect in viral replication was detected in the cells in a primary infection (Figure 5B).

In the follow-up studies, using *ex vivo* cultures of primary CD4+ T cells derived from virally controlled people with HIV-1 (PWH) provided by the Comprehensive NeuroHIV Center (CNHC), we demonstrated that Tat produced upon viral rebound induced CRISPR-MOGS expression, ultimately resulting in the release of non-infectious virions that limit the spread of the virus to uninfected cells (Figures 5E–5G). Importantly, although in control-treated cells the virus-induced syncytia (Figure 5H, top) were readily observed, they were completely absent in cells treated with Tat-inducible CRISPR-MOGS (Figure 5H, bottom). Moreover, results from DNA assay showed significantly lower levels of DNA per equal number of cells in CRISPR-MOGS-treated cells than the control cells (Figure 5I). A combination of lower level and infectivity of rebounded virus derived from Tat-inducible CRISPR-MOGS-treated CD4+ T cells resulted in a drastic decrease in the level of secondary infection compared with virus rebounded from control cells (Figure 5J). Finally, results from the western blot showed the overall decrease in the level of viral protein and more importantly, the appearance of the larger size viral envelope protein exhibiting SaCas9 reduced MOGS in the cells (Figure 5K).

Cooperative interaction of CRISPR-MOGS and CRISPR-HIV in the elimination of HIV-1 infection

To investigate the combinatory effect of CRISPR designed for editing of the *MOGS* gene for impeding viral entry along with the CRISPR engineered for targeting and excising segments of the integrated proviral DNA (CRISPR-HIV),[30] the control or RNP-CRISPR-MOGS-treated Jurkat cells were infected with HIV-1$_{NL4-3-GFP-P2A-nef}$ as before. Again, CRISPR-MOGS treatment had no significant effect on the level of primary viral replication (Figures 6A and 6B), although the shift in the migration of env glycoprotein was evident (Figure 6C). Next, supernatants from the control and the CRISPR-MOGS-treated primary infected cells were used for the secondary infection of HutR5 cells followed by the RNP treatment armed with CRISPR-HIV complex. The CRISPR-HIV-mediated excision of the integrated proviral DNA in HutR5 was verified using PCR genotyping. The appearance of the 198 and 532 bp amplicons indicated the removal of the intervening DNA fragments positioned between the 5'-LTR to Gag and Gag to 3'-LTR, respectively (Figure 6D).[30] The percent of the HutR5 infected cells (identified by GFP+ cells) and the level of viral load in the media (determined by p24) along with the status of the viral envelope protein (Figures 6E–6G), all together point to the functional cooperativity between the CRISPR-mediated inactivation of MOGS and the excision of HIV-1 proviral DNA in mitigating viral replication during the secondary HIV-1 infection of human T lymphocytes.

Next, we adapted this strategy to *ex vivo* T cell cultures prepared from the PWH (P02, P03, and P05) whose viral loads spontaneously rebounded. As shown in Figures 6H and 6I, a single treatment with CRISPR-MOGS decreased the level of MOGS production along with the appearance of larger glycoprotein and a decrease in the secondary viral infection. Lower levels of secondary infections were also observed when rebound virus derived from CRISPR-HIV only treated was used (Figure 6I). Importantly, combined treatments of the CD4+ T cells with CRISPR-MOGS and CRISPR-HIV-1 further declined, albeit to various levels, the production of the infectious viral particles. The different declines in viral levels between T cell cultures from different donors might be the result of different viral loads and alternatively, variability in the efficiency of the delivery of CRISPR.

DISCUSSION

Mutations in the gene encoding MOGS cause the rare congenital disorder of glycosylation type II (CDG-II).[31–33] Remarkably, people with this disorder have no clinical evidence of reoccurring viral infections. Cells derived from people with CDG-II show markedly reduced susceptibility to infection with glycosylation-dependent enveloped viruses like influenza and HIV-1 but not to non-enveloped viruses (adenovirus, poliovirus) or glycosylation-independent enveloped viruses (vaccinia virus).[28] Furthermore, iminosugars, glucose mimetic glucosidase inhibitors, showed a broad spectrum antiviral activity *in vitro* against multiple enveloped viruses like herpes, hepatitis b, hepatitis c, west Nile, dengue Ebola, and coronaviruses including SARS-CoV-2.[34–37] Thus, the role of MOGS in refining the glycan is suspected to be critical for optimal glycosylation of the viral envelope protein and the morphogenesis of pathogenic HIV virions. Under this assumption, glucosidase inhibitors (e.g., SC-48334, Zavesca, miglustat, MDL 28,574A, celgosivir, Bu-CAST) have been evaluated in clinical trials against HIV. The global application of pharmacologic inhibitors revealed unexpected, yet noticeable side effects including

Figure 6. A combination of CRISPR-MOGS and CRISPR-HIV treatments leads to improved virus clearance from *in vitro* infected T cell lines and primary PWH-derived CD4+ T cells

(A) GFP-flow cytometry analysis of HIV-1$_{NL4-3-GFP}$ infection in WT and RNP-CRISPR-Cas9/MOGSgRNA-treated Jurkat cells. (B) HIV-1 gag p24 ELISA results for supernatants collected from cells in (A). (C) Immunoblot analysis of HIV-1 gp160 and MOGS in the same cells. HIV-1 p55 and α-tubulin were used as infection and loading controls. (D) PCR genotyping of CRISPR-Cas9-mediated 5'-LTR-gag and gag-3'-LTR excision of HIV-1 genome observed in HutR5 T-lymphoid cells infected with supernatants derived from cells in (A) and electroporated with Cas9 only (lines 1 and 2) or Cas9/LTR1gRNA + Cas9/GagDgRNA RNP complexes (lines 3 and 4). For 5' LTR-Gag PCR, both full-length 1,200 bp long and CRISPR-cleaved/end-joined 198-bp-long truncated amplicons are detected. For Gag-3'LTR PCR only CRISPR-cleaved/end-joined 532-bp-long truncated amplicon is shown. (E) GFP-flow cytometry analysis of HIV-1$_{NL4-3-GFP}$ infection in the same cells. (F) HIV-1 gag p24 ELISA results for supernatants collected from cells in (E). (G) Immunoblot analysis of HIV-1 gp160 and MOGS in the same cells. HIV-1 p55 and α-tubulin were used as infection and loading controls. (H) Immunoblot analysis of HIV-1 gp160 and MOGS in untransfected, RNP-CRISPR-MOGS, RNP-CRISPR-LTR1/GagD, or RNP-CRISPR-MOGS+RNP-CRISPR-LTR1/GagD treated primary human CD4+ T cells isolated from PBMCs derived from three different people living with HIV (PLWH). HIV-1 p55 and α-tubulin were used as infection and loading controls. (I) ddPCR analysis of viral DNA in the HutR5 cells incubated with supernatant as shown in (H) as a percentage of viral DNA copies detected in control cells. One-way ANOVA and Dunnett's multiple-comparisons test was used in (E) and (F). ****$p < 0.0001$.
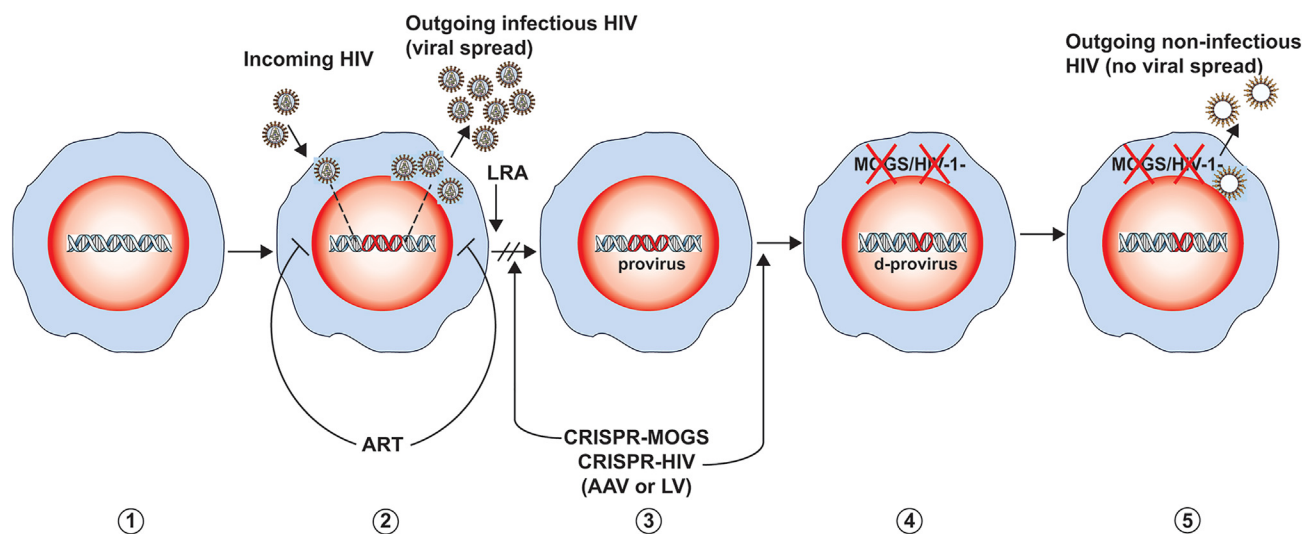
Figure 7. Graphic illustration of CRISPR-mediated mitigation of HIV-1 infection by editing of MOGS and HIV-1 proviral DNA

(1) Uninfected cells. (2) Infection with HIV-1 followed by internalization and integration of viral DNA and replication of infectious virus that can be ceased upon treatment with ART. (3) The treatment with a latency-reversing agent and/or ART removal results in reactivation of latent virus and production of Tat that potentiates CRISPR-MOGS and CRISPR-HIV-1 that are sequentially delivered by transduction with Tat-inducible Cas9/MOGS gRNA and Cas9/HIV-1 gRNA LV or AAV. (4) Suppression of MOGS and excision of segments of proviral DNA leads to defective proviral DNA (d-provirus). (5) Limited production of non-infectious HIV-1 due to aberrant pattern of env glycosylation and defective viral genome.

intestinal distress and osmotic diarrhea,[38–43] in part because of the widespread application of the compound that non-specifically suppressed host glucosidases. Regardless, the beneficial impact of the path for the suppression of viral entry to host was deemed a powerful strategy for antiviral therapy and required a more specific approach toward the suppression of MOGS in the infected cells. As such, we developed a genetic approach that is engineered to inactivate MOGS gene expression by DNA editing that is exclusive to the immune cells containing replication competent, latent HIV-1. We developed a functional pathway whereby activation of the silent virus and the production of the viral protein, Tat, stimulate CRISPR gene editing apparatus that is delivered to the cells.[29] This strategy is aimed at editing of MOGS gene and is designed for the perturbation of glycan configuration of the HIV-1 envelope protein that eventually results in the production of non-infectious virions. Thus, it is reasonable to predict that, in a clinical setting, after the reactivation of latent proviral DNA by latency-reversing agents (LRAs), and the expression of Tat, when ART treatment is interrupted, the overall outcome will be the appearance of non-infectious virus with no ability to spread after rebound from the reservoir. Indeed, the combination treatment with CRISPR designed to excise a segment of proviral DNA, yet having no effect on Tat production, further contributes to the elimination of non-infectious viral particles. As noted, the strategy that is described recruits the critically important HIV-1 protein, Tat, for its replication to initiate a cascade of events that lead to the auto-elimination of virus in the cells.

Importantly, limiting CRISPR gene editing to Tat-expressing and thus HIV-1 infected cells provides an additional level of safety as it was reported that CRISPR deletions are prone to induce p53-related perturbations of cells,[44,45] may impair cell viability and result in complex rearrangements of chromosomes.[46,24] On a different, yet related note, it is postulated that glycosylation of the Env protein functions as a shield to protect the virus against immune-mediated cell defense. Thus, by interfering with the formation of this barrier, newly replicated viral particles may become more susceptible for serving as targets for elimination by the immune cells.[47,48] Therefore, it is plausible to speculate that non-infectious viral progeny may offer a new pathway for the development of a prophylactic vaccine from a weakened, immunogenic viral particles. One may also speculate that the appearance of the inactive, non-infectious viral particles may stimulate the immune system to overcome remaining infectious virus that may escape from elimination by CRISPR-HIV. Thus, the outcome may eventually lead to permanent elimination of HIV-1 in PWH and protects them from re-infection.

In conclusion, here, we propose a proof-of-principle design of a novel and safe strategy that begins with the interruption of ART for control of viremia followed by treatment with LRAs to stimulate the expression of CRISPR that is tailored for elimination of HIV-1 and inactivation of MOGS (Figure 7).

MATERIALS AND METHODS
Cell culture
HEK293T cells (American Type Culture Collection, Manassas, VA) and TZM-bl cells (obtained through the NIH HIV Reagent Program, Division of AIDS, National Institute of Allergy and Infectious Diseases [NIAID], NIH: TZM-bl cells, ARP-8129, contributed by Dr. John C. Kappes and Dr. Xiaoyun Wu)[15,16] were cultured in high-glucose

DMEM supplemented with 10% fetal bovine serum (FBS) and gentamicin (10 μg/mL). Jurkat cells (clone E6, TIB-152; ATCC), HutR5 cells (transformed human T cell line Hut78 stably transduced with CCR5, a gift from Dr. KewalRamani),[49] U1 cells (obtained through the NIH HIV Reagent Program, Division of AIDS, NIAID, NIH: anti-human CD34 hybridoma [PR18], ARP-165, contributed by Dr. Thomas Folks),[20,50,51] J1.1 cells (obtained through the NIH HIV Reagent Program, Division of AIDS, NIAID, NIH: HIV-1 lymphadenopathy-associated virus [LAV]-infected Jurkat E6 cells [J1.1], ARP-1340, contributed by Dr. Thomas Folks),[20,21] and ACH-2 cells (obtained through the NIH HIV Reagent Program, Division of AIDS, NIAID, NIH: ACH-2 cells, ARP-349, contributed by Dr. Thomas Folks)[20,22] were cultured in RPMI medium containing 10% FBS and gentamicin (10 μg/mL) (Sigma-Aldrich, St. Louis, MO). Peripheral blood mononuclear cells (PBMCs) were isolated from whole blood by gradient centrifugation on Ficoll-Paque for 30 min at $600 \times g$ followed by isolation of CD4+ T cells using EasySep Human CD4+ T Cell Isolation Kit (STEMCELL Technologies, Seattle, WA) and then were stimulated with ImmunoCult Human CD3/CD28 T cell activator (STEMCELL Technologies) for 3 days in RPMI with 10% FBS and gentamicin (10 μg/mL) supplemented with human recombinant interleukin-2 (rIL-2) at a concentration of 30 ng/mL (STEMCELL Technologies). Fresh media were exchanged every 2–3 days.

Design of gRNAs and construction of CRISPR-SaCas9-MOGS-A/MOGS-B expression plasmid

The Benchling CRISPR guides designer tool (https://www.benchling.com) was used to screen sequence of human *MOGS* (GeneBank NG_008922.1) gene for possible gRNA protospacer regions followed by SauCas9 specific NNGRR(N) PAM. A pair of gRNAs was selected to introduce an 1,187 bp deletion in the coding sequence of the *MOGS* gene (Figure S2A). Next, a pair of oligonucleotides with 5′-CACC and 3′-AAAC Bsa1 overhangs was obtained from Integrated DNA Technologies (Coralville, IA), annealed, phosphorylated, and ligated into BsaI digested, dephosphorylated pX601-AAV-CMV: NLS-SaCas9-NLS-3xHA-bGHpA; U6::BsaI-single guide RNA (sgRNA) (a gift from Feng Zhang via Addgene, plasmid #61591). For multiplex gRNA cloning, the target pX601-SauCas9-MOGS-B vector was linearized with EcoRI and KpnI, and the insertion fragment (U6-MOGS-A-RNA scaffold) was produced via PCR using the primer pair T795/T796 with a mutation of the 3′-end KpnI site (for further addition of new sgRNAs) and the pX601-SauCas9-MOGS-A vector as the template. After purification, the linearized vector and the insertion PCR product were ligated using an In-Fusion HD Cloning Kit (Takara Bio USA, San Jose, CA). The positive duplex sgRNA-expressing pX601-SauCas9-MOGS-A+MOGS-B clones were identified by double digestion with NotI and BamHI or EcoRI and verified using Sanger sequencing. The same strategy was used to clone a single MOGST4 gRNA into pX601 vector.

Generation the MOGS– single-cell clones

TZM-bl cells were co-transfected with pX601-MOGS-AB and pKLV-U6gRNA-EF(Bbs1)-PGKpuro2ABFP (Addgene 62348, to provide puromycin selection marker). Next day puromycin (1 μg/mL) was added

and cells were grown for a week. Surviving cells were plated in a 96-well plate at a density of 1 cell/well/200 μL of growth medium and clonally expanded for 3 weeks. Finally, expanded clones were screened using PCR-genotyping for the excision of exons 1 and 2 of MOGS gene. Jurkat MOGS– mixed cell population was purchased from Synthego (Redwood City, CA) and clonally expanded in a round-bottom 96-well plates for 3 weeks. Next, expanded clones were screened using PCR genotyping for the presence of indel mutations in exon 2 of MOGS gene. U1, J1.1, ACH1, and HEK293T cells were electroporated with ribonucleoprotein complexes composed of recombinant SaCas9 (Aldevron, Fargo, ND) and synthetic MOGST4 gRNA (Synthego). After two days, transfected cells were clonally expanded and screened as described above for Jurkat cells.

In vitro HIV-1 infections

HEK293T cells were transfected using $CaPO_4$ precipitation method in the presence of chloroquine (50 μM) with 25 μg of pNL4-3-GFP-P2A-Nef[29] or pNL4-3-BAL-GFP GFP (a gift from Dr. Christopher Aiken, Vanderbilt University Medical Center, Nashville, TN) 2.5×10^6 cells/100 mm dish. The next day, medium was replaced, and 24 and 48 h later, supernatants were collected, clarified at 3,000 rpm for 10 min, filtered through a 0.45 μm filter, and concentrated using ultracentrifugation for 2 h with 20% sucrose cushion. Viral pellets were resuspended in Hank's basic salt solution (HBSS) by gentle agitation overnight and aliquoted. Viral titers were measured using GFP-flow cytometry in HutR5 cells. For primary infections, target cells were incubated with HIV-1$_{NL4-3-GFP-P2A-Nef}$ or HIV-1$_{NL4-3-BAL-GFP}$ reporter virus at a multiplicity of infection (MOI) of 0.25 for 4 h in growth medium then inoculum was removed, cells washed twice with PBS and resuspended in growth medium. For secondary infection HutR5 cells were incubated with supernatants from primary infections overnight, next cells were washed twice with PBS and resuspended in fresh growth medium.

RNP-CRISPR electroporations

Guide RNAs were coupled individually with SaCas9 by adding 2.2 μL of sNLS-SaCas9-sNLS Nuclease (10 μg/mL = 80 μM; Aldevron) to 6 μL of synthetic gRNA (60 μM, CRISPRevolution Custom RNA [modified], Synthego) in 11.8 μL of electroporation Buffer R (Neon; Life Technologies, Carlsbad, CA, USA). The molar ratio when incubating was 1:2 (9 μM:18 μM) SaCas9:gRNAs. The mixtures were incubated individually for 10 min at room temperature (RT), then combined and added to 2.5×10^6 of target cells in 200 μL Buffer R. Cells were then mixed gently and electroporated using the Neon Electroporation Device set to 1,400 V, 1×30 ms impulse with 100 μL Neon tip. Cells were immediately plated in 4 mL of pre-warmed growth medium.

Nucleic acid extractions and standard PCR and RT-PCR assays

Genomic DNA was extracted from cells using NucleoSpin Tissue kit (Macherey-Nagel Inc., Bethlehem, PA). Briefly, the cell pellet was resuspended in 200 μL T1 followed by adding of 25 μL Proteinase K solution (2.5 mg/mL) and overnight incubation at 55°C. The next day, 20 μL RNAse A (10 mg/mL) was added, and samples were incubated

for 5 min at RT. The extraction was then completed according to the manufacturer's instructions. Genomic DNA was eluted in 100 μL elution buffer (5 mM Tris/HCl [pH 8.5]) and quantified using Nanodrop. For standard PCRs (Table S2), 250 ng extracted DNA was subjected to PCR using Terra PCR Direct polymerase mix (Takara Bio) under the following PCR conditions: 98°C for 2 min, 30 cycles (98°C for 10 s, 60°C for 15 s, and 68°C for 120 s), 68°C for 7 min using 1st-round primers followed by nested PCR using diluted 1st-round PCR. Next, amplicons extracted from the agarose gels were sent for Sanger sequencing (Azenta, South Plainfield, NJ). For RT PCR, Monarch Total RNA Miniprep kit (New England BioLabs Inc., Ipswich, MA) was used for RNA extraction and Protoscript II First Strand cDNA Synthesis Kit for reverse transcription. For gRNA expression screening specific reverse primer (pX601gRNA scaffold/R; Table S1) was used in RT reaction followed by standard PCR using target LTR or Gag sense oligos as forward primers (Table S1) and agarose gel electrophoresis. For checking saCas9 mRNA expression oligo-dT primer mix was used in RT and cDNA was subjected to PCR using saCas9 specific primer pairs and β-actin as a reference (Table S1). Sanger sequencing results were analyzed using Clustal Omega (EMBL-EBI) multiple sequence alignment tool and Sequence Scanner Software 2 (Applied Biosystems).

ddPCR for quantification of HIV-1 DNA
ddPCR was performed on the basis of the water-oil emulsion droplet technology, using the ddPCR Supermix for Probes reagents in the QX200 Droplet Digital PCR system (Bio-Rad Laboratories, Hercules, CA). For quantification of HIV-1 DNA, the eluted cellular DNA was PCR amplified using Taqman sets targeting HIV-ψ and as a reference human TERT gene (Table S1). A total of 50–100 ng DNA was used as template for ddPCR amplifications with thermal cycling conditions used 98°C for 5 min, 45 cycles (98°C for 15 s, 60°C for 30 s). Data acquisition and analysis were done using QX200 droplet reader and QuantaSoft software provided with the instrument.

Antibodies and western blot
One million cells were lysed with RIPA buffer (25 mM Trizma base [pH 7.6], 150 mM NaCl, 1% NP-40, 1% sodium deoxycholate, 0.1% SDS) containing a protease inhibitor cocktail (Sigma-Aldrich) and electrophoresed on 8% or 10% polyacrylamide SDS-PAGE gels using 1X Tris-Glycine-SDS running buffer. Gels were transferred onto 0.22 μm Odyssey nitrocellulose membranes (LI-COR, P/N 926-31092) using the Bio-Rad Trans-Blot Turbo Transfer System, blocked for 1 h in 5% milk + Tris-buffered saline-Tween 20 (TBS-T). Membranes were probed with primary antibody in appropriate blocking buffer overnight at 4°C. Membranes were washed three times with TBS-T for 10 min at RT and probed with secondary antibody in the same blocking buffer used for primary antibody at 1:10,000 dilution for 60 min at RT. Blots were washed as before. Images were acquired using the Odyssey CLx Imaging System (LI-COR). Antibodies used were glucosidase 1 (C11) (sc-374006; Santa Cruz Biotechnology, Dallas, TX), gp160 (13390; NIH AIDS Reagent Program), α-tubulin (32-2500; Life Technologies), HIV (3957; NIH AIDS Reagent Program), HIV-1 gp120 (2343; NIH AIDS Reagent Program), SaCas9

(A01951; GenScript, Piscataway, NJ). For PNGnase F or Endo H treatment, denatured protein lysates were incubated for 1 h at 37°C with 500 units PNGase F or Endo H (New England BioLabs Inc.) prior to acrylamide gel electrophoresis.

Cell proliferation, viability, cell cycle, and apoptosis assays
Jurkat and U1 WT and MOGS− cells were plated at the density of 1×10^5 cells/mL. An aliquot of cells was stained with propidium iodide (2 μg/mL) for 1 min for four consecutive days and analyzed using Guava MiniCyte 8 flow cytometer (Luminex, Austin, TX). For the cell cycle analysis 10^6 cells were fixed with 70% ethanol (cells were resuspended in 1 mL of $1\times$ PBS and then dropwise added into 4 mL cold 88% ethanol) and stored at 4°C. The next day, fixed cells were spun down, washed twice with PBS, and resuspended in staining buffer containing propidium iodide (20 μg/mL) and RNAse A (200 μg/mL) for 30 min at 37°C and then placed on ice and analyzed using Guava MiniCyte 8 flow cytometer. Apoptotic assay was performed using Guava Nexin Reagent (Luminex). Briefly, 10^5 cells in 100 μL ($1\times$ PBS, 1% FBS) were mixed with 100 μL Guava Nexin Reagent and incubated for 20 min at RT in the dark and then analyzed using Guava MiniCyte 8 flow cytometer.

Construction of pPapi-LTR-SaCas9_MOGST4 plasmid
The U6-MOGST4 guide RNA expression cassette was sub-cloned from pX601-MOGST4 plasmid into pPapi (a gift from John Doench and David Root via Addgene plasmid #96921) vector by PCR using Acc651-U6 F and Scaffold-BstBI R primers (Table S2) resulting in pPapi-MOGST4 plasmid. Next, the original EF 1a promoter was replaced with the LTR (−80/+66) promoter using NheI/XbaI and AgeI restriction sites. The final construct was named as pPapi-LTR-SaCas9_MOGST4.

Electron microscopy
HutR5 T cells were incubated for 1 h with equal titers of virus-containing supernatants collected from MOGS+ or MOGS− J1.1 cells (300 ng Gag p24/10^7 cells). After 1 h, cells were spun down and fixed in 2% glutaraldehyde for 1 h at RT (10^7 cells/10 mL). Next, cells were treated with OsO_4, stained with 0.5% uranyl acetate, pelleted in 2% agarose, dehydrated in a dilution series of acetone/water, and embedded in Spur's resin (Electron Microscopy Sciences). The sections were examined with a JEOL JEM1010 transmission electron microscope (TEM) fitted with a side-mounted AMT XR-50 5Mpx CCD camera. Whole-cell images were taken with 2,100× direct magnification. Cell membrane and cytosolic regions were imaged with 15,000× direct magnification.

MALDI-glycan imaging
Virus-containing supernatants from ACH-2 (WT, MOGS− C17 and C20) and J1.1 (WT, MOGS− C8, and C12) induced with TNF-α (50 ng/mL) overnight were ultracentrifuged (25,000 × g, 2 h, 4°C, 20% sucrose cushion), and the viral pellets were resuspended in Urea Lysis Buffer (9 M urea, 50 mM Tris [pH 8], 100 U/mL Thermo Universal Nuclease; Life Technologies). Purified viruses were spotted on nitrocellulose as we have done with purified protein previously.[25]

Cell-based N-glycan imaging was adapted from previously published protocols.[26,27,52] J1.1 and U1 cells suspended in PBS were plated over chambered hydrogel-coated slides (Nexterion Slide H) and incubated for 1 h, allowing a monolayer of cells to covalently bind. The excess cell suspension was removed, and the slide dried in a desiccator. Bound cells were fixed with 10% neutral buffered formalin for 20 min. Cell chambers were removed, and cells were washed with Carnoy's solution (10% glacial acetic acid, 30% chloroform, 60% ethanol) (10 min × 2), 100% ethanol (2 min × 2), and high-performance liquid chromatography (HPLC)-grade water (3 min × 2). PNGase F PRIME (0.1 μg/μL in HPLC water) was sprayed onto the slide using an M5 TM-Sprayer (HTX Technologies) for 10 passes at 25 μL/min, 1,200 mm/min, 45°C, 3 mm spacing between passes with 10 psi nitrogen gas. The slide was incubated for 2 h at 37°C in a humidity chamber. MALDI matrix α-cyano-4-hydroxycinnamic acid (CHCA; 7 mg/mL in 50% acetonitrile/49.9% water/0.1% trifluoroacetic acid) was applied using the same M5 TM- Sprayer for 10 passes at 70 μL/min, 1,300 mm/min, 79°C, 2.5 mm spacing between passes with 10 psi nitrogen gas. Ammonium phosphate monobasic (5 mM) was applied after matrix application for two passes at 70 μL/min, 1300 mm/min, 60°C, and 3 mm spacing between passes with 10 psi nitrogen gas. A dual-source timsTOF flex MALDI-QTOF mass spectrometer (Bruker) was used to conduct N-glycan analysis. Cells were imaged using a SmartBeam 3D laser, operating at 10,000 Hz using an M5 small smart beam at a 100 μm laser spot size. Images were taken at a 150 μm raster with 600 laser shots per pixel. Cells were analyzed with an m/z range of 700–4,000 in positive ion mode. SCiLS Lab 2022a (Bruker) was used to analyze the data generated. Mass spectra were normalized to total ion count.

β-lactamase viral entry assay

To generate HIV-1 virions containing active β-lactamase for use in viral entry assays the pMM310 vector (obtained through the NIH HIV Reagent Program, Division of AIDS, NIAID, NIH: HIV-1 YU2 Vpr β-lactamase expression vector [pMM310], ARP-11444, contributed by Dr. Michael Miller [Merck Research Laboratories])[23] was co-transfected into HEK293T WT or MOGS− (Clone M4) cells together with pNL4-3 HIV-1 genome containing plasmids. After 48 h the supernatants containing viral particles packaged with Vpr-β-lactamase fusion protein were harvested and tittered by Gag p24 ELISA. Next, TZM-bl cells were plated in 384-well plates at density 2×10^4 cells/well and incubated with equal titers of HIV-1 virions containing active β-lactamase (4 ng Gag p24/well). After 2 h CFF2-AM substrate (Life Technologies) to final concentration of 1 ng/mL was added and incubated for another 2 h. Then cells were fixed with 2% paraformaldehyde (20 min) and analyzed using high content image analysis. Viral entry was quantified in a confocal Operetta CLS from PerkinElmer. Acquisition data from the 384 well plate was performed using a 40× water immersion objective. Twenty fields were acquired per well and three planes per field, corresponding to one-quarter of the well. Total cells stained with CCF2-AM were detected using the green channel (488/555 nm), and viral fusion-positive cells were detected using the blue channel (400/430 nm). Data analysis was performed using the Harmony 4.8 software from PerkinElmer. Spe-

cific parameters for total cell identification and viral infection were established using a positive control (TZM-bl-pMM310) (Figure S9). Positive viral entry cells were calculated using the maximum intensity signal per cell, both TZM-bl-HIV BaL WT and TZM-bl-HIV BaL M4 were normalized against the signal from the control (TZM-bl-Untr). The percentage of viral entry was calculated as the number of cleaved-CCF2-AM-positive cells (blue) in each condition out of the total number of cells identified per well (green, uncleaved-CCF2-AM-positive) (Figure 3B).

LV vector production

Lipofectamine 3000 (Life Technologies) was used for lentiviral production. Specifically, HEK293T cells at about 75% confluency were transfected in 100 mm cell culture plates with 3 μg pCMV-VSV-G (a gift from Bob Weinberg via Addgene, plasmid #8484), 6 μg psPAX2 (a gift from Didier Trono via Addgene, plasmid #12260) and 8.5 μg pPapi-LTR-SaCas9_MOGST4 according to manufacturer protocol. First viral supernatant was collected 24 h post-transfection, which was combined with second viral supernatant collected about 52 h post-transfection. The combined viral supernatants were first centrifuged at 2000 rpm to remove cell debris, then syringe filtered through a 0.45 μm filter. After the clean-up, lentivirus was aliquoted and stored in a −80°C freezer until use. The lack of recombination between lentiviral vector truncated 5′-LTR/3″-LTRs and HIV-1 LTR −80/+60 Tat-inducible promoter in pPapi-LTR-SaCas9_-MOGST4 vector was verified after packaging and after transduction using qRT-PCRs and ddPCR, assays respectively (Figure S14).

Statistical analysis

Data were analyzed using Prism 9.0 (GraphPad, La Jolla, CA) and are presented as mean ± SEM. Experiments were performed using a minimum of two biologically distinct replicates. One-way ANOVA and Dunnett's multiple comparisons test were used for statistical analyses. For comparisons of two groups, a two-tailed unpaired t test was used.

DATA AVAILABILITY

The data supporting the findings of this study are available from the corresponding author upon reasonable request. Source data for all figures will be provided upon request.

SUPPLEMENTAL INFORMATION

Supplemental information can be found online at https://doi.org/10.1016/j.omtn.2023.04.027.

manuscript. We appreciate Cynthia Papaleo for the assembly of data and preparation of this manuscript. This work was made possible by grants awarded by the NIH to K.K. and T.H.B. (P30MH092177) and in part by W. W. Smith Charitable Trust to R.K. (grant A-1902). This research was supported (in part) by the CRISPR for Cure Martin Delaney Collaboratory for HIV cure UM1 AI164568-02 and co-funded by NIAID, the National Institute of Mental Health (NIMH), the National Institute on Drug Abuse (NIDA), the National Institute of Neurological Disorders and Stroke (NINDS), the National Institute of Diabetes and Digestive and Kidney Diseases (NIDDK), and the National Heart, Lung, and Blood Institute (NHLBI).

AUTHOR CONTRIBUTIONS

K.K., R.K., C.R.Y.C., and C.M.B. conceived the idea and conducted direct experiments. H.L., C.C., S.L., D.K.S., R.K., A.M., M.F., C.B., S.G., and J.D. conducted and performed experiments. K.K., T.H.B., R.K., C.C., T.J.C., J.G., A.M., C.M.B., and C.B. analyzed data. K.K., R.K., T.H.B., S.A., C.C., and C.M.B. prepared, commented on, and edited the manuscript.

DECLARATION OF INTERESTS

K.K. and R.K. from Temple University and C.M.B. and C.R.Y.C. from Children's National Health System are named inventors on patents that cover the viral gene editing technology for MOGS that is the subject of this article. C.M.B. and C.R.Y.C. hold patent 9,885,021 related to MOGS editing of HIV-specific T cell therapies licensed by Mana Therapeutics. C.M.B. and C.R.Y.C. are scientific cofounders of Mana Therapeutics and serve on its scientific advisory board (SAB). In addition to the foregoing interests, K.K. is a co-founder, board member (observer), and chief scientific adviser and holds equity in Excision Biotherapeutics, a biotech startup that has licensed the viral gene editing technology from Temple University for commercial development and clinical trials. T.H.B. holds equity in Excision Biotherapeutics and is a member of its SAB. T.J.C. and J.G. are members of Excision Biotherapeutics, who provided advice and assisted in the design of some part of experimental quality control of the gRNAs. All other authors have no interests to disclose.

REFERENCES

1. Kwong, P.D., Wyatt, R., Robinson, J., Sweet, R.W., Sodroski, J., and Hendrickson, W.A. (1998). Structure of an HIV gp120 envelope glycoprotein in complex with the CD4 receptor and a neutralizing human antibody. Nature 393, 648–659.

2. Ray, N., and Doms, R.W. (2006). HIV-1 coreceptors and their inhibitors. Curr. Top. Microbiol. Immunol. 303, 97–120.

3. Sattentau, Q.J. (1992). CD4 activation of HIV fusion. Int. J. Cell Clon. 10, 323–332.

4. Chen, B. (2019). Molecular mechanism of HIV-1 entry. Trends Microbiol. 27, 878–891.

5. Binley, J.M., Ban, Y.E.A., Crooks, E.T., Eggink, D., Osawa, K., Schief, W.R., and Sanders, R.W. (2010). Role of complex carbohydrates in human immunodeficiency virus type 1 infection and resistance to antibody neutralization. J. Virol. 84, 5637–5655.

6. Blough, H.A., Pauwels, R., De Clercq, E., Cogniaux, J., Sprecher-Goldberger, S., and Thiry, L. (1986). Glycosylation inhibitors block the expression of LAV/HTLV-III (HIV) glycoproteins. Biochem. Biophys. Res. Commun. 141, 33–38.

7. Coss, K.P., Vasiljevic, S., Pritchard, L.K., Krumm, S.A., Glaze, M., Madzorera, S., Moore, P.L., Crispin, M., and Doores, K.J. (2016). HIV-1 glycan density drives the persistence of the mannose patch within an infected individual. J. Virol. 90, 11132–11144.

8. Fischer, P.B., Collin, M., Karlsson, G.B., James, W., Butters, T.D., Davis, S.J., Gordon, S., Dwek, R.A., and Platt, F.M. (1995). The alpha-glucosidase inhibitor N-butyldeoxynojirimycin inhibits human immunodeficiency virus entry at the level of post-CD4 binding. J. Virol. 69, 5791–5797.

9. Behrens, A.J., Vasiljevic, S., Pritchard, L.K., Harvey, D.J., Andev, R.S., Krumm, S.A., Struwe, W.B., Cupo, A., Kumar, A., Zitzmann, N., et al. (2016). Composition and antigenic effects of individual glycan sites of a trimeric HIV-1 envelope g lycoprotein. Cell Rep. 14, 2695–2706.

10. Cao, L., Pauthner, M., Andrabi, R., Rantalainen, K., Berndsen, Z., Diedrich, J.K., Menis, S., Sok, D., Bastidas, R., Park, S.K.R., et al. (2018). Differential processing of HIV envelope glycans on the virus and soluble recombinant trimer. Nat. Commun. 9, 3693.

11. Crispin, M., Ward, A.B., and Wilson, I.A. (2018). Structure and immune recognition of the HIV glycan shield. Annu. Rev. Biophys. 47, 499–523.

12. Struwe, W.B., Chertova, E., Allen, J.D., Seabright, G.E., Watanabe, Y., Harvey, D.J., Medina-Ramirez, M., Roser, J.D., Smith, R., Westcott, D., et al. (2018). Site-specific glycosylation of virion-derived HIV-1 Env is mimicked by a soluble trimeric immunogen. Cell Rep. 24, 1958–1966.e5.

13. Helenius, A., and Aebi, M. (2001). Intracellular functions of N-linked glycans. Science 291, 2364–2369.

14. Reily, C., Stewart, T.J., Renfrow, M.B., and Novak, J. (2019). Glycosylation in health and disease. Nat. Rev. Nephrol. 15, 346–366.

15. Platt, E.J., Wehrly, K., Kuhmann, S.E., Chesebro, B., and Kabat, D. (1998). Effects of CCR5 and CD4 cell surface concentrations on infections by macrophagetropic isolates of human immunodeficiency virus type 1. J. Virol. 72, 2855–2864.

16. Wei, X., Decker, J.M., Liu, H., Zhang, Z., Arani, R.B., Kilby, J.M., Saag, M.S., Wu, X., Shaw, G.M., and Kappes, J.C. (2002). Emergence of resistant human immunodeficiency virus type 1 in patients receiving fusion inhibitor (T-20) monotherapy. Antimicrob. Agents Chemother. 46, 1896–1905.

17. Murray, S.M., Zhang, Y., Douek, D.C., and Sekaly, R.P. (2020). Myeloid cells enriched for dendritic cell popultion from people living with HIV have altered gene expression not restored by antiretroviral therapy. Front. Immunol. 11, 261.

18. Rappaport, J., and Volsky, D.J. (2015). Role of the macrophage in HIV-associated neurocognitive disorders and other comorvidities in patients on effective antiretroviral treatment. J. Neurovirol. 21, 235–241.

19. Cohn, L.B., Chomont, N., and Deeks, S.G. (2020). The Biology of the HIV-1 latent reservoir and implications for cure strategies. Cell Host Microbe 27, 519–530.

20. Symons, J., Chopra, A., Malatinkova, E., De Spiegelaere, W., Leary, S., Cooper, D., Abana, C.O., Rhodes, A., Rezaei, S.D., Vandekerckhove, L., et al. (2017). HIV integration sites in latently infected cell lines: evidence of ongoing replication. Retrovirology 14, 2. Erratum in: Retrovirology.

21. Perez, V.L., Rowe, T., Justement, J.S., Butera, S.T., June, C.H., and Folks, T.M. (1991). An HIV-1-infected T cell clone defective in IL-2 production and Ca2+ mobilization after CD3 stimulation. J. Immunol. 147, 3145–3148.

22. Clouse, K.A., Powell, D., Washington, I., Poli, G., Strebel, K., Farrar, W., Barstad, P., Kovacs, J., Fauci, A.S., and Folks, T.M. (1989). Monokine regulation of human immunodeficiency virus-1 expression in a chronically infected human T cell clone. J. Immunol. 142, 431–438.

23. Cavrois, M., De Noronha, C., and Greene, W.C. (2002). A sensitive and specific enzyme-based assay detecting HIV-1 virion fusion in primary T lymphocytes. Nat. Biotechnol. 20, 1151–1154.

24. Boutin, J., Cappellen, D., Rosier, J., Amintas, S., Dabernat, S., Bedel, A., and Moreau-Gaudry, F. (2022). ON-target adverse events of CRISPR-cas9 Nuclease: more chaotic than expected. CRISPR J 5, 19–30. https://doi.org/10.1089/crispr.2021.0120.

25. Black, A.P., Liang, H., West, C.A., Wang, M., Herrera, H.P., Haab, B.B., Angel, P.M., Drake, R.R., and Mehta, A.S. (2019). A novel mass spectrometry platform for multiplexed N-glycoprotein biomarker discovery from patient biofluids by antibody panel based N-glycan imaging. Anal. Chem. 91, 8429–8435.

26. Blaschke, C.R.K., Black, A.P., Mehta, A.S., Angel, P.M., and Drake, R.R. (2020). Rapid N-Glycan Profiling of Serum and Plasma by a Novel slide-based imaging mass spectrometry workflow. J. Am. Soc. Mass Spectrom. 31, 2511–2520.

27. Powers, T.W., Jones, E.E., Betesh, L.R., Romano, P.R., Gao, P., Copland, J.A., Mehta, A.S., and Drake, R.R. (2013). Matrix assisted laser desorption ionization imaging mass spectrometry workflow for spatial profiling analysis of N-linked glycan expression in tissues. Anal. Chem. 85, 9799–9806.

28. Moore, S.E., and Spiro, R.G. (1990). Demonstration that Golgi endo-alpha-D-mannosidase provides a glucosidase-independent pathway for the formation of complex N-linked oligosaccharides of glycoproteins. J. Biol. Chem. 265, 13104–13112.

29. Kaminski, R., Chen, Y., Salkind, J., Bella, R., Young, W.B., Ferrante, P., Karn, J., Malcolm, T., Hu, W., and Khalili, K. (2016). Negative feedback regulation of HIV-1 by gene editing strategy. Sci. Rep. 6, 31527.

30. Dash, P.K., Kaminski, R., Bella, R., Su, H., Mathews, S., Ahooyi, T.M., Chen, C., Mancuso, P., Sariyer, R., Ferrante, P., et al. (2019). Sequential LASER ART and CRISPR treatments eliminate HIV-1 in a subset of infected humanized mice. Nat. Commun. 10, 2753. https://doi.org/10.1038/s41467-019-10366-y.

31. Chang, J., Block, T.M., and Guo, J.T. (2013). Antiviral therapies targeting host ER alpha-glucosidases: current status and future directions. Antivir. Res. 99, 251–260.

32. Grunewald, S., Matthijs, G., and Jaeken, J. (2002). Congenital disorders of glycosylation: a review. Pediatr. Res. 52, 618–624.

33. Sadat, M.A., Moir, S., Chun, T.W., Lusso, P., Kaplan, G., Wolfe, L., Memoli, M.J., He, M., Vega, H., Kim, L.J.Y., et al. (2014). Glycosylation, hypogammaglobulinemia, and resistance to viral infections. N. Engl. J. Med. 370, 1615–1625.

34. Alonzi, D.S., Scott, K.A., Dwek, R.A., and Zitzmann, N. (2017). Iminosugar antivirals: the therapeutic sweet spot. Biochem. Soc. Trans. 45, 571–582.

35. Casas-Sanchez, A., Romero-Ramirez, A., Hargreaves, E., Ellis, C.C., Grajeda, B.I., Estevao, I.L., Patterson, E.I., Hughes, G.L., Almeida, I.C., Zech, T., and Acosta-Serrano, Á. (2021). Inhibition of protein N- glycosylation blocks SARS-CoV-2 infection. mBio 13, e0371821.

36. Chang, J., Block, T.M., and Guo, J.T. (2015). Viral resistance of MOGS-CDG patients implies a broad- spectrum strategy against acute virus infections. Antivir. Ther. 20, 257–259.

37. Watanabe, Y., Bowden, T.A., Wilson, I.A., and Crispin, M. (2019). Exploitation of glycosylation in enveloped virus pathobiology. Biochim. Biophys. Acta Gen. Subj. 1863, 1480–1497.

38. Fischl, M.A., Resnick, L., Coombs, R., Kremer, A.B., Pottage, J.C., Jr., Fass, R.J., Fife, K.H., Powderly, W.G., Collier, A.C., Aspinall, R.L., et al. (1994). The safety and efficacy of combination N-butyl- deoxynojirimycin (SC-48334) and zidovudine in patients with HIV-1 infection and 200-500 CD4 cells/mm3. J. Acquir. Immune Defic. Syndr. 7, 139–147.

39. Hoechst, M.R. (1996). A randomized, double-blind active-controlled, dose-ranging study of the safety and efficacy of chronically administered MDL 28,574A in the treatment of HIV-infected patients. NLM identifier: NCT0002151.

40. Hoechst, M.R. (1996). A study of the safety and efficacy of chronically administered MDL 28,574A in the treatment of HIV-infected patients. NLM identifier: NCT0002150.

41. Searle, G.D. (1992). Initial Phase II Efficacy and Safety Study of SC-48334 Administered in Combination with Low-Dose Zidovudine (AZT) to Symptomatic HIV-1 Infected Patients with = or > 200 to = or < 500 CD4+ Cells/mm3. NLM Identifier: NCT0001993.

42. Searle, G.D. (1993). Phase II Study of the Safety and Surrogate Marker Efficacy of Butyldeoxynojirimycin (SC-48334) and AZT in Symptomatic HIV-1 Infected Patients with 200- 500 CD4+ Cells/mm3. NLM Identifier: NCT0002079.

43. Tierney, M., Pottage, J., Kessler, H., Fischl, M., Richman, D., Merigan, T., Powderly, W., Smith, S., Karim, A., Sherman, J., et al. (1995). The tolerability and pharmacokinetics of N-butyl-deoxynojirimycin in patients with advanced HIV disease (ACTG 100). The AIDS clinical trials group (ACTG) of the national institute of allergy and infectious diseases. J. Acquir. Immune Defic. Syndr. Hum. Retrovirol. 10, 549–553.

44. Haapaniemi, E., Botla, S., Persson, J., Schmierer, B., and Taipale, J. (2018). CRISPR-Cas9 genome editing induces a p53-mediated DNA damage response. Nat. Med. 24, 927–930. https://doi.org/10.1038/s41591-018-0049-z.

45. Enache, O.M., Rendo, V., Abdusamad, M., Lam, D., Davison, D., Pal, S., Currimjee, N., Hess, J., Pantel, S., Nag, A., et al. (2020). Cas9 activates the p53 pathway and selects for p53-inactivating mutations. Nat. Genet. 52, 662–668. https://doi.org/10.1038/s41588-020-0623-4.

46. Turchiano, G., Andrieux, G., Klermund, J., Blattner, G., Pennucci, V., El Gaz, M., Monaco, G., Poddar, S., Mussolino, C., Cornu, T.I., et al. (2021). Quantitative evaluation of chromosomal rearrangements in gene-edited human stem cells by CAST-Seq. Cell Stem Cell 28, 1136–1147.e5. https://doi.org/10.1016/j.stem.2021.02.002.

47. He, S., and Wu, Y. (2019). Relationships between HIV-mediated chemokine coreceptor signaling, cofilin hyperactivation, viral tropism switch and HIV-mediated CD4 depletion. Curr. HIV Res. 17, 388–396.

48. Sun, L., Paschall, A.V., Middleton, D.R., Ishihara, M., Ozdilek, A., Wantuch, P.L., Aceil, J., Duke, J.A., LaBranche, C.C., Tiemeyer, M., and Avci, F.Y. (2020). Glycopeptide epitope facilitates HIV-1 envelope specific humoral immune responses by eliciting T cell help. Nat. Commun. 11, 2550.

49. Wu, L., Martin, T.D., Vazeux, R., Unutmaz, D., and KewalRamani, V.N. (2002). Functional evaluation of DC- SIGN monoclonal antibodies reveals DC-SIGN interactions with ICAM-3 do not promote human immunodeficiency virus type 1 transmission. J. Virol. 76, 5905–5914.

50. Hu, W., Kaminski, R., Yang, F., Zhang, Y., Cosentino, L., Li, F., Luo, B., Alvarez-Carbonell, D., Garcia-Mesa, Y., Karn, J., et al. (2014). RNA-directed gene editing specifically eradicates latent and prevents new HIV-1 infection. Proc. Natl. Acad. Sci. USA 111, 11461–11466.

51. Folks, T.M., Justement, J., Kinter, A., Dinarello, C.A., and Fauci, A.S. (1987). Cytokine-induced expression of HIV-1 in a chronically infected promonocyte cell line. Science 238, 800–802.

52. Angel, P.M., Saunders, J., Clift, C.L., White-Gilbertson, S., Voelkel-Johnson, C., Yeh, E., Mehta, A., and Drake, R.R. (2019). A rapid array-based approach to N-Glycan profiling of cultured cells. J. Proteome Res. 18, 3630–3639.